STUDY OF BOND BETWEEN EPOXY, STEEL REINFORCING BARS AND CONCRETE AFFECTED BY ALKALI-SILICA REACTION

Félix-Antoine Villemure[1], Mathieu Fiset[1], Josée Bastien[1], Denis Mitchell[2], Benoît Fournier[1], Benoît Bissonnette[1]

[1]Université Laval, Quebec City, QC, CANADA

[2]McGill University, Montreal, QC, CANADA

Abstract

Installation of drilled-in epoxy bonded reinforcing bars is generally an effective strengthening method for deficient concrete structures. However, this method of rehabilitation has largely been studied and tested on sound concrete elements, i.e. without any pathological damage, which raises the question of bond capabilities in existing damaged elements. This investigation studies the influence of alkali-silica reaction (ASR) on the capacity of epoxy bonded anchors. ASR, which is very common in eastern Canada, results from the chemical reaction between the alkali hydroxides in the concrete's pore solution and some siliceous mineral phases in the aggregates. Pull-out tests on epoxy bonded anchors having embedded lengths of four times the bar diameter (Ø = 16 mm) have demonstrated a drop in bond strength when concrete is affected by ASR. In addition, the study revealed that the progression of concrete expansion due to ASR, leads to a confinement of the epoxy bonded anchor and increases the bond strength. These conclusions are therefore considered for the development of a model for the design of epoxy bonded anchors in existing concrete infrastructure affected by ASR.

Keywords: post-installed bonded anchors, pullout test, alkali-silica reaction (ASR)

1 INTRODUCTION

The collapse of the Concorde overpass on September 30th, 2006 in Laval (Canada), demonstrated how brittle shear failures can occur in thick concrete slabs without shear reinforcement after many years in service. Many similar deficient structures were built between the 50s and 70s in Canada, and require particular attention due to the effects of concrete degradation that constitutes a risk to public safety.

Following this event, several research projects have been performed at Université Laval with the common objective to investigate different methods of post-installed shear reinforcement. Loading tests on shear-critical thick concrete slab specimens indicated that the most efficient strengthening method consisted of post-installed epoxy bonded steel bars [1,2]. Only a few studies have investigated the behavior of post-installed bonded bars [3,4,5]; however, the epoxy bonded anchors were only tested on elements of sound concrete, that is without any pathological damage. Since many structures that need shear strengthening are damaged by concrete degradation, it is important to investigate the effect of a damaged concrete matrix (cracks) on the bond strength of epoxy bonded anchors.

This research project, compares the bond strength of epoxy bonded anchors embedded in sound concrete and as well as in concrete affected by alkali-silica reaction (ASR). Swelling of alkali-silica gel inside the aggregate, caused by ASR, leads to the formation of cracks in the aggregate particles and, eventually, inside the cementitious matrix. These cracks may have an effect on bond strength. The effects of ASR progression (crack development and expansion increase) on the bond strength after the embedment of the epoxy bonded anchors were also studied.

2 EXPERIMENTAL PROGRAM

2.1 Materials and mix designs

Ten (10) concrete specimens, 350 x 350 x 350 mm in size, divided into four (4) specimens of sound concrete (specimens S) and six (6) specimens of concrete with a potential for ASR (specimens A and D), were cast with very similar concrete mixes. An extremely reactive coarse aggregate (high amount of reactive silica particles) from New Mexico and a high-alkali Portland cement were selected in order to accelerate the development of ASR. The petrographic facies and potentially reactive phases of the New Mexico aggregate are shown in TABLE 1 [6]. A lithium nitrate admixture was added to the sound concrete mix to inhibit the initiation of ASR while NaOH was added to the concrete mix

with a potential for ASR, to accelerate the reaction. The water to cement ratio of the two concrete mixes was 0.47. The concrete mix designs are presented in TABLE 2.

2.2 Concrete conditioning and installation of epoxy bonded anchors

After 28 days of moist curing at room temperature, tests specimens S, A and D were stored in hermetic containers, in a room at 38°C. Relative humidity inside the containers was kept ≥ 95% during conditioning. The volumetric deformations caused by ASR were monitored, in directions parallel and perpendicular to the concrete casting plane, using a linear comparator on embedded studs. The conditioning was stopped after 200 days, when lateral expansion of specimens A and D reached approximatively 0.15% (parallel to the concrete casting plane). Lateral expansion was chosen as the limiting criterion because cracks parallel to the bar axis at the concrete/adhesive interface significantly reduce the bond resistance [7]. Specimens S were removed from conditioning at the same time, while their lateral expansion was approximatively 0%.

Epoxy bonded anchors were installed in the test specimens in drilled holes of 19 mm diameter. Steel reinforcing bars of 15M metric size (bar diameter Ø = 16 mm) were installed with an embedded length of 4Ø (~64 mm). The installation of the epoxy bonded anchors was designed so that the longitudinal axis of the steel reinforcing bars was always perpendicular to the concrete casting plane. An anti-corrosion paint was applied to the external part of steel reinforcing bars embedded in specimens D. After the installation of anchors, specimens S and A were tested, while specimens D were returned to conditioning and monitored for another 100 days to study the effects of increased ASR damage.

2.3 Test procedure

The experimental setup was based on the ASTM E488-10 confined pullout test, as shown in FIGURE 1. To ensure uniaxial tensile loading, a ball joint was used to keep the reinforcing bars parallel to the load cell. The load was applied through the reinforcing bar at a rate of 2 mm/min and the tested specimen was supported on the concrete block upper face by a supporting plate and steel rods. This design was chosen because it allows a better control of the failure mode i.e. to avoid a concrete cover splitting or concrete cone failure since these failure modes don't allow to determine the full bond-slip relationship. FIGURE 1 also shows that the steel reinforcing bar is not bonded to concrete along the top 100 mm of embedment, which reduces the effect of confinement pressure caused by the top supporting plate [8]. The elongation of the steel reinforcing bars was monitored by two extensometers (unbonded length), while the relative displacement between concrete surfaces and the steel reinforcing bars (slip - s) was monitored by four linear variable differential transformers (LVDTs).

3 RESULTS

3.1 Expansion and damage

Progression of the concrete expansion measured perpendicular to the bar axis (conditioning at 38°C and RH ≥ 95%) is presented in FIGURE 2a. The shade in graphs (a) marks out the maximum and minimum expansions. It can be observed that the expansion of concrete specimens S is negligible, as expected, indicating that the lithium has inhibited the ASR expansion. For specimens A and D affected by ASR, the increasing rate of the concrete expansion is almost constant during all the conditioning period.

Signs of damage associated with ASR were observed in specimens A and D. The opened cracks in the coarse aggregate particles with reaction product, cracking in the cement paste with reaction product, air voids filled with reaction product and reaction rims around the reactive aggregate particles confirmed that the expansion of specimens A and D resulted from ASR. The reaction product observed in cracks and voids shows the typical texture of alkali-silica gel. This damage is shown in FIGURE 3 from a sample of specimen A concrete.

3.2 Mechanical properties

The steel reinforcing bars were tested in uniaxial tension (ASTM E08-04, E111-04) and the mechanical properties are as follows: yield strength, f_y of 456 MPa, ultimate strength, f_u of 567 MPa, strain hardening strain, ε_{sh} of 0.023, strain at rupture, ε_u of 0.175 and Young's modulus, E_s of 190 GPa.

Concrete cores were drilled from the tested specimens perpendicular to the concrete casting plane (parallel to the axis of the bar during pullout tests) to determine the in-situ concrete mechanical properties. Compressive strength tests, tensile strength tests and Young's modulus have been

determined in accordance with ASTM C1231-14, C496-11 and C469-14, respectively. These properties are summarized in TABLE 3. It is clear that the mechanical properties have decreased with the increased expansion caused by ASR. The compressive strength and Young's modulus were particularly affected by ASR. The compressive strength and the Young's modulus have decreased 31% and 55%, respectively, between specimens S and A. Specimen S and D experienced similar decreases of these properties with a drop of 43% and 56%, respectively. A significant decrease of Young's modulus was noted for specimens A at 0.15% of expansion. Similar values of tensile strength and Young's modulus were obtained for specimens A and D despite the increase of the expansion for specimens D. The decrease of tensile strength and Young's modulus seemed to have reached a threshold.

Fernandez et al. [4] suggested using Eq. (1) to account for the effect of the concrete strength in determining the bond strength. For comparison purpose between tests, bond stresses are compared for the same concrete compressive strength f_c of 20 MPa, and the equivalent bond stress, τ_{b0}, are used in the following analysis of pullout tests. The experimental bond stress is calculated by dividing the applied load by the full embedded length (average bond stress) according to Eq. (2), where Ø is the bar diameter, σ_{sL} is the bar loaded end axial stress and L is the embedded length.

$$\tau_b = \tau_{b0}\left(\frac{f_c}{20}\right)^{0.1} \quad \text{(in MPa)} \tag{1}$$

$$\tau_b = \frac{\phi\sigma_{sL}}{4L} \tag{2}$$

3.3 Pullout tests

The loading setup resulted in debonding failures for all specimens; no concrete cone failures or splitting failures were observed. Typical failures are shown in FIGURE 4. The study of pulled-out bars demonstrates that the failure surface is between the epoxy and the concrete interface or through the adhesive for all tested specimens. No significant concrete remained bonded to the pulled-out bars.

FIGURE 2b shows the equivalent bond stress, τ_{b0}, according to the loaded end slip, s, of the post-installed epoxy bonded anchors and FIGURE 5 shows the applied stress according to the bar slip. The shade in graphs marks out the maximum and minimum stresses. It can be seen in FIGURE 5 that the bars of specimens S and D reached the bar yielding strength while bars of specimens A debonded before yielding. In FIGURE 2b, it can be seen that the median bond strength of specimens S was about 30 MPa. By comparing with specimens A, it can be observed that the median experienced slightly lower bond strengths (about 29 MPa) than for specimens S, while the shade shows a significant lower bond strength (about 20 MPa). Similar scatter can be observed for specimens D, with median bond strength of 31 MPa and lower bond strength of 24 MPa. Based on the median, the slip at failure is also lower for the specimens A (about 2 mm) than for specimens S and for specimens D (about 4 mm). One specimen A and one specimen D exhibited premature failure (s < 1 mm).

It is interesting to note that the median bond strength of the specimens D (31 MPa) is higher than the median bond strength observed on specimens S with sound concrete (30 MPa). Thus, anchors installed in concrete with ASR reduce the bond strength, but the progression of ASR can actually increase the bond strength. This increase may be due to the expansion of the concrete caused by ASR and producing a confinement pressure. It has been reported that confinement pressure applied perpendicularly to the bar axis has a significant effect on the bond strength [5,9]. The scatter of the results was probably a result of the probability of encountering a crack in the embedment length of the anchor. The presence of cracks in the periphery of the anchor reduces the area available for the transfer of forces between the epoxy resin and the concrete matrix, causing a drop in the mechanical capacity of the anchor.

4 MODELING

4.1 Description of the model

Axial bar stress and strain along the bar are presented in FIGURE 6. It can be observed that these quantities vary along the bar embedded length and are function of the bond stress [10]. In a finite elements (FE) model, it is assumed that the adhesive thickness is thin and, thus, the bonding agent carries only shear force between the bar and the concrete. For bonded bars, the axial stress has to be transferred from the bar to the surrounding concrete by the bonding agent. The bar axial stress at the free extremity $\sigma_{s(x=0)} = 0$ and the bar slip s is free $s_{(x=0)} = s_0 > 0$. It can also be observed that the bond stress and the slip distributions are not constant along the embedment length. The bond stress is a function of the slip between the bar and the surrounding concrete, which is function of the strains

and the axial stresses in the two materials. From equilibrium and compatibility of deformations (see FIGURE 6), the variation of the bar slip *ds* is defined by Eq. (3) as the difference between the steel strain ε_s and the concrete strain ε_c along the bonded length dx.

$$ds = (\varepsilon_s - \varepsilon_c)\,dx \tag{3}$$

Assuming uniform axial stress along *dx* follows the relation in Eq. (4) between the concrete axial stress σ_c, the steel axial stress σ_s and the bond stress τ, where ρ_s is the ratio between the bar area and the concrete area (A_s/A_c).

$$d\sigma_s = \frac{d\sigma_c}{\rho_s} = \frac{4}{\phi}\tau dx \tag{4}$$

With the appropriate bond-slip relationship and the assumed boundary conditions, all the concrete and steel axial strains and stresses, as well as the bond distribution, can be determined by assuming the bar stress and bar slip at the loaded bar end, as shown in FIGURE 6a. This model enables to solve these equations by assuming the applied slip to an initial value and the bar stress to an assumed value at the loaded bar end and by dividing the bar in 1000 elements. The bond stress along the first element is determined from the bond-slip relationship and the applied slip (slip at the top of the element). Then, the variation of the steel and the concrete stresses are determined from the Eq. (4) . The summation of $d\sigma$ with Eq. (5) for concrete and steel enables to determine the stresses in each element, which is considered constant along an element. Then, the material strains are determined from the stress-strain relationship of materials of Eq. (6) and (7) and the slip at the following node can be found from Eq. (3) (slip at the bottom of the element). This procedure is repeated for all elements, the solution at the bar extremity is compared to the boundary conditions and the applied stress is modified until convergence. Repeating the procedure until the failure of the bar enables the full embedded bar behavior to be determined.

The concrete and steel materials stress-strain relationships are determined as follow [11]. Since the concrete stress is small in compression or below the tensile strength, the concrete is assumed to be elastic.

$$\sigma_{i+1} = \sigma_i + d\sigma \tag{5}$$

$$\varepsilon_s = \begin{cases} \sigma_s / E_s & \sigma_s \le f_y \\ \varepsilon_u - (\varepsilon_u - \varepsilon_{sh})\left(\dfrac{\sigma_s - f_u}{f_y - f_u}\right)^{1/p} & f_y \le \sigma_s \le f_u \end{cases} \tag{6}$$

$$\varepsilon_c = \sigma_c / E_c \tag{7}$$

Where $p = E_{sh}\,(\varepsilon_u - \varepsilon_{sh}) / (f_u - f_y)$ and E_{sh} is the initial strain hardening modulus taken from experimental results as 3.5 GPa. The appropriate bond-slip relationship was determined for short embedded bars experiencing elastic stress ($\sigma_s < f_y$) bonded in sound concrete (expansion of 0%) (FIGURE 7a). The tests were similar to the ones previously presented. It was found that the best fit bond-slip relationship were in accordance with the expression from Cosenza et al. [12] (FIGURE 7a). The best fit parameters are presented in TABLE 4.

$$s > s_2 \quad \tau = \tau_b - (\tau_b - \tau_f)\left(\frac{s - s_2}{s_3 - s_2}\right) \ge \tau_f \tag{8}$$

$$s \le s_2 \quad \tau = \tau_b \left(1 - e^{(-s/s_r)}\right)^{\beta} \tag{9}$$

According to the fib Model Code [9], for large tensile strains, the bond is reduced by the lateral contraction of the bar, whereas it increases for large compressive strain. To incorporate the influence of steel strain above yielding, the bond coefficient K_b is used to reduce the equivalent bond strength τ_{b0} in Eq. (1) for the bond stress relationship. Fernandez-Ruiz et al. [14] proposed the following coefficients for steel-concrete interface. It is assumed that the K_b coefficient can be used for bonded anchorages.

$$K_b = \exp\left(10(\varepsilon_y - \varepsilon_s)\right) \tag{10}$$

$$\Omega_w = 1 - 10(w/\varnothing) \tag{11}$$

$$\Omega_p = 1 - \tanh\left(2\sigma_p / f_c\right) \tag{12}$$

To incorporate the ASR effect in the model, the lower capacities of the concrete are taken into account by reducing the concrete Young's modulus in Eq. (7) and the concrete compressive strength in Eq. (1) according to the measured values (Table 3). Moreover, Mahrenholtz [3] proposed that the equivalent bond strength τ_{b0} of Eq. (1) be multiplied by Ω_w, given by Eq. (11), to incorporate the

effect of cracks crossing the embedded bar, with a crack width, w, parallel to the bar axis (FIGURE 7b). Mahrenholtz [3] and fib Model Code [9] also reported that transverse pressure applied perpendicularly to the bar axis may increase (confinement) or decrease (tension) the bond strength of a cast-in-place anchor. In the current study, it is expected that specimens D may experience confinement pressure due to the higher ASR expansion. To take into account the confinement pressure σ_p, fib Model Code [9] suggests that the equivalent bond strength τ_{b0} of Eq. (1) be multiplied by Eq. (12). It is proposed that these factors can be used to take into account the concrete cracking and the confinement stress caused by ASR in post-installed bonded anchors.

4.2 Modeling results

The boundary conditions used in the model are presented in FIGURE 6. Prediction of the applied axial bar stress, $\sigma_{s,FE,}$ versus bar slip, s, responses are presented and compared to the experimental results in FIGURE 5 and TABLE 6. For all specimens, it can be seen that the model predicts the yielding of the bar before the debonding failure. On average, the model predicts almost the same load at failure as the experimental values ($\sigma_{sL,FE}$ / $\sigma_{sL,exp}$ = 0.996, cov = 0.041). The use of the yielding coefficient K_b is therefore appropriated for post-installed anchors.

For specimens A, previous studies have found that a crack width of 0.24 mm best fits the behaviour of post-installed anchors with a 5Ø (~80 mm) embedded length with 0.20% of concrete expansion [13]. This equivalent crack width leads to a reduction of about 15% of the bond strength (Eq. (11)). Using this crack width for 4Ø (~64 mm) embedded bars in the current study gives also good predictions of the specimen responses. The ratio between the predicted maximum stress $\sigma_{s,FE}$ and the experimental results $\sigma_{s,exp}$ is 0.964 (cov = 0.039) for specimens A. This shows that using the equivalent crack approach with a crack width of 0.24 mm gives good prediction of the specimen A with 0.15% of concrete expansion and 4Ø embedded length.

For specimens D experiencing an increase of the ASR effects, the concrete expansion increased by about 0.10% in average, i.e. from 0.15% to about 0.25%. Other pullout tests performed on bars with 5Ø embedded lengths by Villemure et al. [13] resulted in an equivalent crack width of 0.30 mm for 0.25% of concrete expansion (see FIGURE 7c). This equivalent crack width leads to a reduction of about 18% of the bond strength (Eq. (11)). Two other analyses are compared in TABLE 5 for specimens D with no confinement pressure (Eq. (12)) and a lower bound equivalent crack width of 0.24 associated with lower ASR effects (specimens A).

It can be seen in Table 5 that omitting the confinement effect and using the lower bound effective crack width leads to an underestimation of the anchor capacity by 64 MPa ($\sigma_{sL,FE}$ / $\sigma_{sL,exp}$ = 0.875, cov = 0.077). As a lower bound, a confining pressure of about 4.1 MPa is required in the model to fit the experimental maximum anchor capacity ($\sigma_{sL,FE}$ / $\sigma_{sL,exp}$ = 1.000, cov = 0.081). By using the estimation of the equivalent crack width based on previous results (FIGURE 7c), it can be seen that a confinement pressure of 5.0 MPa is required to best fit the experimental results (cov = 0.081). By using a crack width of 0.30 mm and a confinement pressure 5.0 MPa, very good predictions of the full anchor behaviour are found, as shown in FIGURE 5. Even by using a lower bound crack width, accounting for confinement pressure is required to fit the experimental results. Thus, according to the model, the effects of the concrete expansion from 0.15 to 0.25% on the bond strength are equivalent to a confinement pressure of 5.0 MPa.

This research shows that considering the reduction of the concrete mechanical properties by Eq. (1) is not sufficient to explain the effects of the ASR on the capacity of post-installed bonded anchors. The bond strength of embedded bars in concrete affected by ASR is also reduced because of the cracking. Moreover, to explain the higher bond strength of embedded bars in concrete experiencing higher levels of concrete expansion due to ASR, the confinement effects have to be taken into account.

5 CONCLUSIONS

Mechanical characterization tests have shown the decrease of compressive strength, tensile strength and Young's modulus with increased expansion caused by ASR. The decrease seemed to have reached a threshold for tensile strength and Young's modulus because similar results were obtained for 0.15% and 0.25% of lateral expansion.

Pullout tests on epoxy bonded anchors embedded in sound concrete and concrete affected by ASR have shown that ASR has an influence on bond strength. A decrease of bond capacity was observed for specimens affected by ASR. Most specimens have shown a slight reduction of bond strength, while one specimen has shown a significant capacity reduction. The same scatter was

observed on specimens after the progression of ASR damage. It was assumed that the decrease of the bond strength was caused by the presence of longitudinal cracks (parallel to the bar axis) in the periphery of the anchor. However, the study revealed that the higher levels of concrete expansion due to ASR (ASR progression), resulted in confinement of the epoxy bonded anchors and increased bond strength.

A finite element model using bond-slip relationships was used to predict the behavior of post-installed, drilled-in anchors, including the capacity. The effects of ASR on the bond-slip behavior was taken into account in the model by using a reduced concrete compressive strength, cracked concrete and confinement pressure. The predictions using the finite element model agreed very well with the experimental results. The analyses and the experimental results indicated that the capacity of post-installed anchors decreases with ASR because of both the decrease of concrete mechanical properties and ASR cracking. This conclusion mainly affects the behaviour of newly installed bonded anchors. After time, the ASR progress and the concrete expansion increases, causing confinement pressure. Even if bond strength decreases by the decreasing of the concrete mechanical properties and the concrete cracking, the confinement pressure may increase the anchor capacity. Eventually, using criteria based on ASR cracking and concrete expansion may be used to predict the capacity of post-installed bonded anchors.

6 ACKNOWLEDGMENTS

This research was supported by the Natural Sciences and Engineering Research Council of Canada (NSERC), by the CREATE-INFRA program and by the Research Center on Concrete Infrastructures (CRIB).

7 REFERENCES

[1] Provencher, P (2011): Renforcement des dalles épaisses en cisaillement (Shear stengthening of concrete thick slabs, in French), Université Laval, Québec, Canada.

[2] Cusson, B (2012): Renforcement des dalles épaisses en cisaillement (Shear stengthening of concrete thick slabs, in French), Université Laval, Québec, Canada.

[3] Eligehausen, R., Cook, R and Appl, J (2006): Behaviour and design of adhesive bonded anchors, ACI Structural Journal, ACI, 103: 822-831.

[4] Fernandez-Ruiz, M, Muttoni, A and Kunz, J (2010): Strengthening of flat slabs against punching shear using post-installed shear reinforcement, ACI Structural Journal, ACI, 107: 434-442.

[5] Mahrenholtz, C (2012): Seismic bond model for concrete reinforcement and the application to column-to-foundation connections, Universität Stuttgart, Stuttgart, Germany.

[6] Villeneuve, V (2011): Détermination de l'endommagement du béton par la méthode pétrographique quantitative (Determination of the concrete damage by the quantitative petrographique method, in French), Université Laval, Québec, Canada.

[7] Eligehausen, R, Balogh, T (1995): Behavior of fasteners loaded in tension in cracked reinforced concrete, ACI Structural Journal, ACI, 92: 365-379.

[8] Appl, J (2009): Tragverhalten von Verbunddübeln unter Zugbelastung (Behaviour of bonded anchors under tensilion loading, in German), Universität Stuttgart, Stuttgart, Germany.

[9] fib - Fédération international du béton (2013) : Model Code for Concrete Structures 2010, fib, Lausanne, Suisse.

[10] Filippou, FC, Popov, EP, Bertero, VV (1983): Modelling of R/C joints under cyclic excitations, Journal of Structural Engineering, ASCE, 109: 2666-2684.

[11] Palermo, D, & Vecchio, FJ (2003): Compression Field Modelling of Reinforced Concrete Subjected to Reversed Loading: Verification, ACI Structural Journal, Vol. 101, No. 2: 155-164

[12] Cosenza, E, Manfredi, G, Realfonzo, R (1997): Behavior and modelling of bond of FRP rebars to concrete, Journal of composites for construction, ASCE, 1: 40-51.

[13] Villemure, FA, Fiset, M, Bastien, J, Mitchell, D and Fournier, B (2015): Effet de la réaction alcalis-silice (RAS) sur l'adhérence des ancrages époxydiques de barres d'armature (Study of epoxy bonded anchors on concrete affected by alkali-silica reaction), Proceeding of the 16th edition of (RF)²B, Lausanne, Switzerland.

[14] Fernández-Ruiz, M; Muttoni, A; Gambarova, PG (2013): Analytical modeling of the pre- and postyield behavior of bond in reinforced concrete, Journal of Structural Engineering, ASCE, 133: 1364-1372

TABLE 1: Petrographic facies and potentially reactive phases of New Mexico aggregate from results of Villeneuve [6].

Facies	*Type*	*Proportion [%] (-14 + 10 mm)*	*Proportion [%] (-20 + 14 mm)*	*Potentially reactive phases*
A	Andesite-basalt	19.0	36.1	Volcanic glass
B	Quartzite	56.7	35.4	Microcrystalline quartz (10%)
C	Granite	18.5	20.1	Microcrystalline quartz (5%) and quartz with undulatory extinction
D	Granitic gneiss	2.8	3.3	Quartz with undulatory extinction
E	Rhyolite	2.6	2.0	Microcrystalline quartz (~20%)
F	Pelite	0.4	3.1	-

TABLE 2: Concrete mixes design (kg/m³).

Components	*Sound concrete*	*Concrete affected by alkali-silica reaction*
Cement	370.0	370.0
Fine aggregate	742.6	742.6
Coarse aggregate	1091.8	1091.8
NaOH	-	0.7
Lithium nitrate ($LiNO_3$)	28.3	-
Water	174.0	174.0
Density	2376.0	2368.2

TABLE 3: Mechanical properties of concrete.

Specimen	S	A	D
Average expansion	0%	0.15%	0.25%
Compressive strength [MPa]	43.6	30.3	24.7
Tensile strength [MPa]	3.1	2.2	2.4
Young's modulus [GPa]	35.1	15.9	15.3

TABLE 4: Parameters for the bond stress relationship of bonded anchorage (refer to Eq. (8) and (9)).

τ_{b0}	τ_b	s_r	β	s_2	τ_f	s_3
32.26 MPa	Eq. (1)	0.323 mm	0.566	2.07 mm	$0.35\tau_b$	11.3 mm

TABLE 5: Average of the experimental and predicted maximum axial bar stress at the bar loaded end.

Specimen	S	A	D		
FE crack width (mm)	0	0.24	0.24	0.24	0.30
FE confinement (MPa)	0	0	0	4.1	5.0
$\sigma_{s.FE}$ (MPa)	509 ± 19	391 ± 42	447 ± 5	511 ± 4	511 ± 4
$\sigma_{s.exp}$ (MPa)	511 ± 44	406 ± 54	511 ± 54		
$\sigma_{s.FE}$ / $\sigma_{s.exp}$	0.996	0.964	0.875	1.000	1.000
Coefficient of variation	0.041	0.039	0.077	0.081	0.081

FIGURE 1: Experimental setup for pullout test.

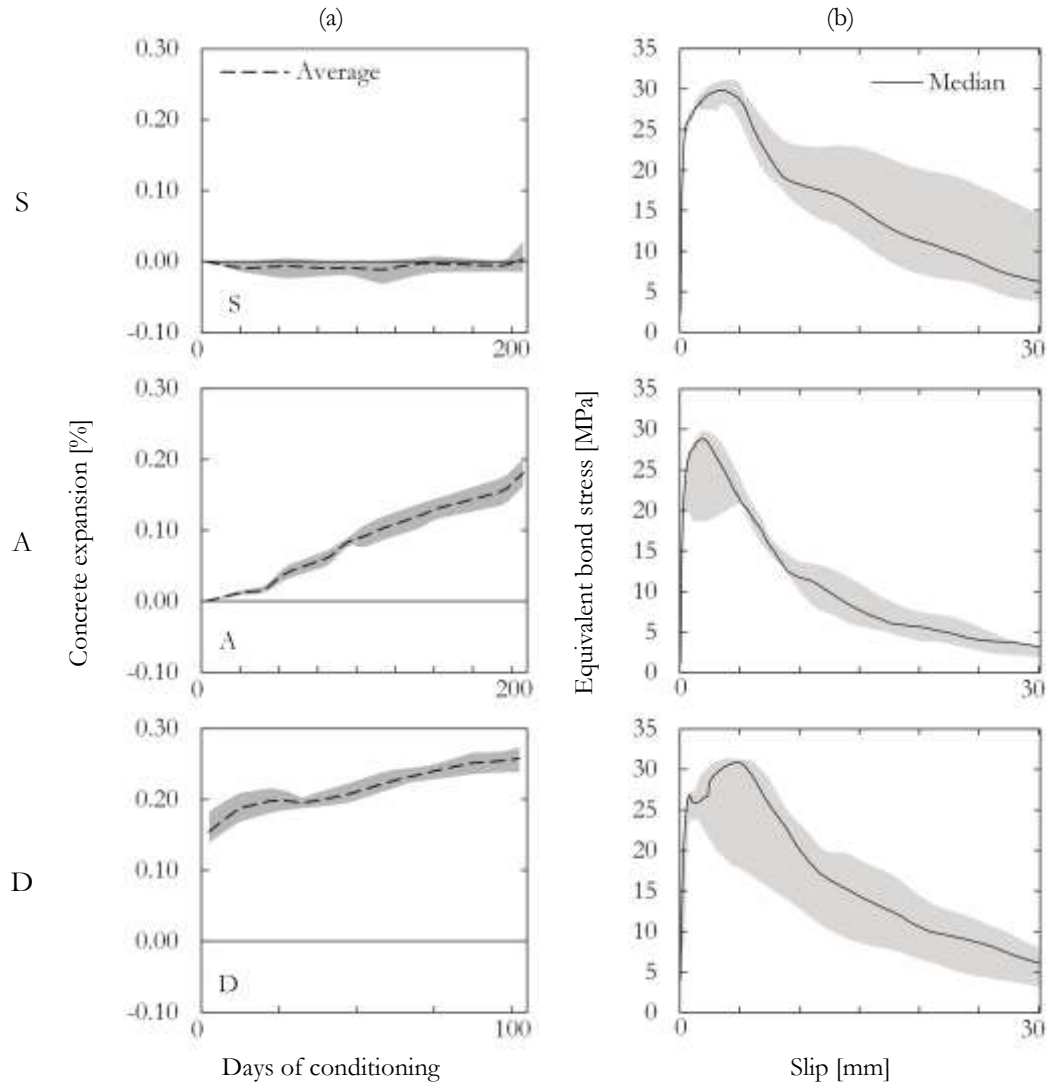

FIGURE 2: (a) Progression of the concrete expansion measured perpendicularly to the bar axis and (b) bond stress according to the epoxy bonded bar loaded end slip. The shade in graphs (a) and (b) marks out the maximum and minimum expansions and bond stresses, respectively.

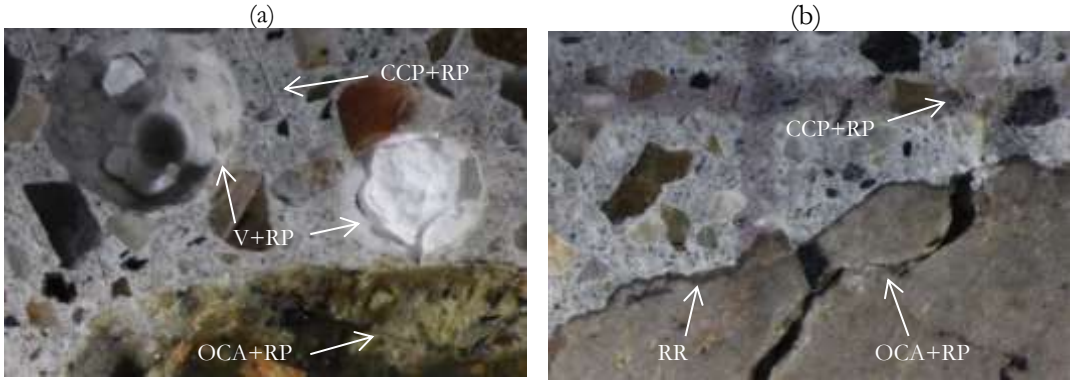

FIGURE 3: Typical damage caused by ASR. (a) Reaction product in air voids (V+RP), opened crack in a coarse aggregate particle with reaction product (OCA+RP) and crack in the cement paste with reaction product (CCP+RP); (b) Reaction rim (RR), opened crack in a coarse aggregate particle with reaction product (OCA+RP) and crack in the cement paste with reaction product (CCP+RP).

FIGURE 4: Typical epoxy bonded anchors after pullout.

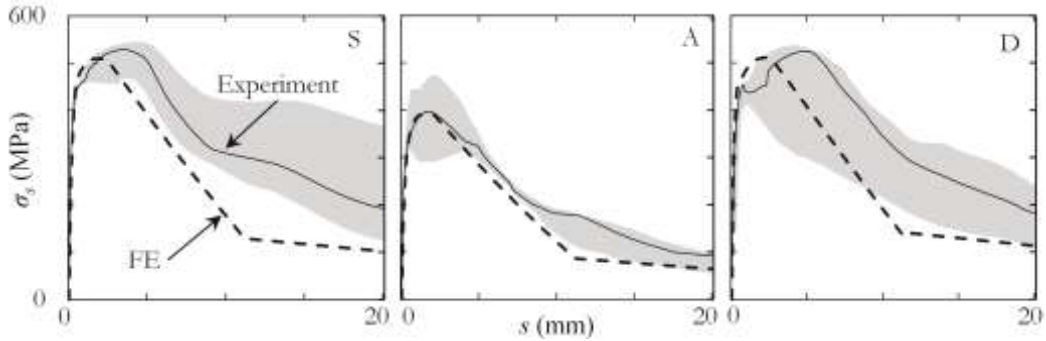

FIGURE 5: Comparison between experimental and FE predictions of the bar loaded end axial stress as a function of the bar loaded end slip, specimens S, A and D.

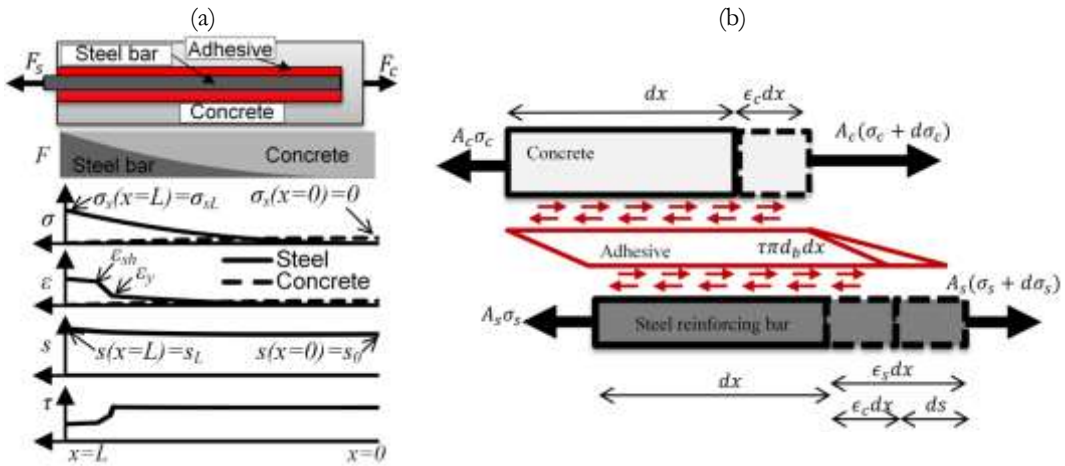

FIGURE 6: Bar stresses and strains (a) along the embedded length and (b) for an element of length *dx*.

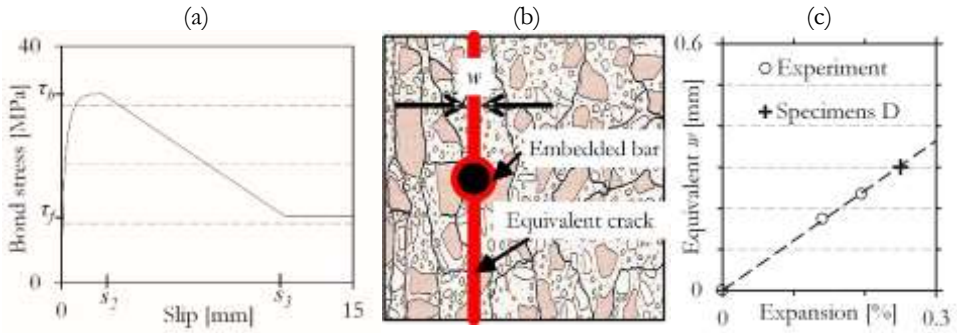

FIGURE 7: (a) Base curve of the epoxy adhesive bond slip relationship, (b) equivalent cracking and (c) extrapolation of the crack with for specimens D from results of Villemure et al. [13].